Journal of Geodynamics 51 (2011) 398–410

Contents lists available at ScienceDirect

Journal of Geodynamics

journal homepage: http://www.elsevier.com/locate/jog

Present-day deformation along the El Pilar Fault in eastern Venezuela: Evidence of creep along a major transform boundary

François Jouanne[a,*], Franck A. Audemard[b], Christian Beck[a], Aurélien Van Welden[a], Reinaldo Ollarves[a,b], Carlos Reinoza[b]

[a] Université de Savoie, LGCA, UMR CNRS 5025, Campus Scientifique, F73376, Le Bourget du Lac, France
[b] Venezuelan Foundation for Seismological Research, FUNVISIS, Final Prolongación Calle Mara, Quinta Funvisis, El Llanito, Caracas 1073, Venezuela

ARTICLE INFO

Article history:
Received 2 June 2010
Received in revised form 3 November 2010
Accepted 3 November 2010
Available online 11 November 2010

Keywords:
Caribbean
El Pilar Fault
GPS
Relative motion
Creep

ABSTRACT

The right-lateral strike-slip El Pilar Fault is one of the major structures that accommodate the relative displacement between the Caribbean and South-America Plates. This fault, which trends East–West along the northeastern Venezuela margin, is a seismogenic source, and shows numerous evidence for active tectonics, including deformation of the Quaternary sediments filling the Cariaco Gulf. Because the main El Pilar Fault strand belongs to a set of strike-slip faults and thrusts between the stable Guyana shield (South) and the Caribbean oceanic floor (North), a GPS network was designed and installed to measure the relative motion of the El Pilar Fault and other faults. The results obtained from the comparison of 2003 and 2005 surveys indicate: (i) a lack of significant displacement (especially shortening) in the Serrania del Interior (Neogene cordillera overthrusted above the Guyana craton), (ii) an eastward displacement (relative to fixed south America plate) up to 22 mm/year of benchmarks located north of the El Pilar Fault.

Velocities simulations using dislocations in an elastic half-space show: (1) the concentration along the El Pilar Fault of the whole Caribbean-South America relative displacement, (2) the existence of an important component of aseismic displacement along the upper part of the El Pilar Fault. Between 12 km depth and the surface, only 40% of displacement is locked for the western segment and 50% for the eastern segment. This last phenomenon may be related to the existence of serpentinite lenses along the fault zone as observed for segments of San Andreas and North Anatolian faults.

1. Geological and geodynamic setting of the El Pilar Fault. Brief introduction

1.1. The Caribbean Chain

Northern Venezuela is bounded by an East-West cordillera, almost 1000 km long, with an eastward prolongation in northern Trinidad (Fig. 1). Different review publications provide detailed geological information (non exhaustive list) on the so-called "Caribbean Chain" and its foreland: the Geological and Structural Map of Venezuela by Bellizzia et al. (1976), the book by González de Juana et al. (1980) and the new geologic shaded relief map of Venezuela by Hackley et al. (2005).

Although northern Venezuela (Perijá Range, Mérida Andes, Caribbean Coast Range) has well recorded Paleozoic and Precambrian evolutions, we will only focus on its Mesozoic–Cenozoic part. Present-day geology (Fig. 2) results from a complex polyphase evolution which developed from West toward East, after the opening of the central Atlantic. The importance of allochtony – southeastward overthrusting – was underlined by Peirson (1965), Menéndez (1966), Bell (1971), Bellizzia (1972), Stéphan (1985) and Beck (1985). In addition, Rod (1956) highlighted the significance of major strike-slip displacements. The south-Caribbean margin formed during the middle-upper Jurassic ocean opening between the North- and South-American Plates (Stéphan et al., 1990). The boundaries of this passive margin were a combination of E-W-trending, northward-dipping, growth normal faults, and of NW-SE transform faults. Inheritance of this pattern strongly influenced the Cenozoic tectonic evolution of the margin, and is guiding the present activity in northeastern Venezuela and Trinidad (Fig. 1). During Cretaceous and Paleogene, different "terranes" from central eastern pacific (island arc, ophiolites, continental microplate) built a complex set of tectonic units stacked by transpression (thrusting and lateral accretion) along the southern transform boundary of the eastward-moving Caribbean Plate. In the Eastern Caribbean Chain (Fig. 2, section B), the metamorphic units are directly in contact with Early Cretaceous-Paleogene platform sediments, while in the western Caribbean Chain (Fig. 2, section A), they overthrust an ancient Paleogene deep sea fan, deformed into an accretionary wedge (a "proto-Barbados Prism"). The Oligocene-Miocene fore-

* Corresponding author. Tel.: +33 479758887.
E-mail address: fjoua@univ-savoie.fr (F. Jouanne).

0264-3707/$ – see front matter © 2010 Elsevier Ltd. All rights reserved.
doi:10.1016/j.jog.2010.11.003

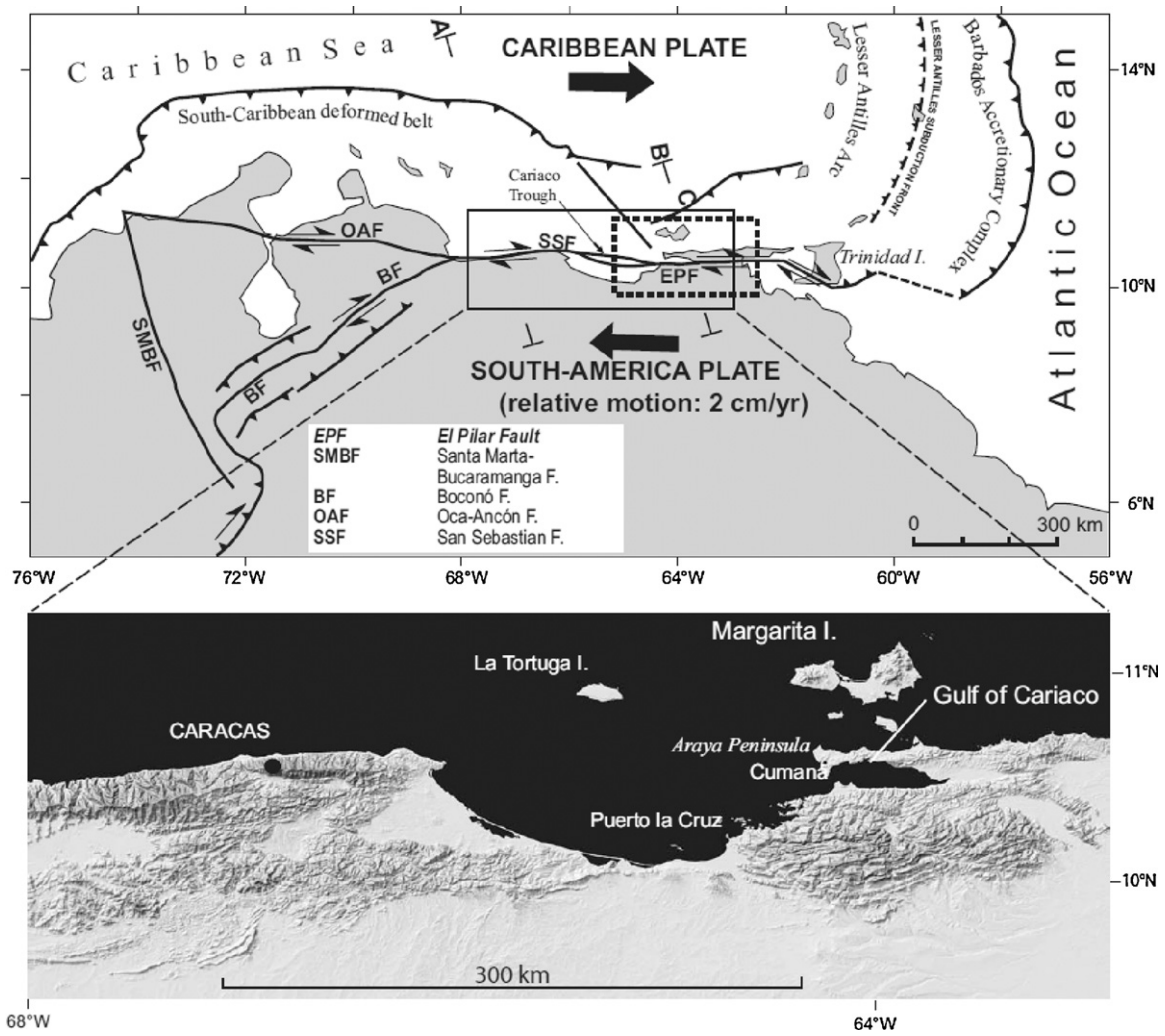

Fig. 1. Geodynamic sketch map of the southeastern Caribbean and morphology of the central and eastern Caribbean Chain (Audemard, 1999; Weber et al., 2001).

land is deeper in the Eastern Chain, with a prominent negative gravimetric signature (Graterol, 1988). In the eastern portion (Fig. 2, section B), the El Pilar Fault tends to separate the outer sedimentary belt from the metamorphic units. Nevertheless, this juxtaposition results from a Neogene overprinting by the E-W strike-slip movement, as Vignali and Vierbuchen (Vignali, 1977; Vierbuchen, 1978) mentioned local overthrusting of Araya–Paria schists on non metamorphosed sedimentary rocks of the Eastern Interior Range. Thus, we image this situation on sections B (Fig. 1), just north of the El Pilar Fault.

1.2. The El Pilar Fault zone

During the Cenozoic, the general kinematics of the Caribbean followed the pattern initiated during the upper Cretaceous: eastward drift of the Caribbean Plate, Atlantic oceanic subduction below the Lesser Antilles volcanic island arc, growth and eastward drift of the Barbados accretionnary complex (Beck et al., 1990). Fig. 1 shows the present-day situation, based on structural analysis, seismology, seismo-tectonics, and GPS measurements (DeMets et al., 2000; Minster and Jordan, 1978; Pérez and Aggarwal, 1981; Audemard et al., 2000; Pérez et al., 2001a,b; Weber et al., 2001). The present-day relative displacement and deformations along northern Venezuela (underlined in red in Fig. 2) can be divided into: major strike slip faults (SW-NE and E-W trending), offshore horizontal N-S to NNW-SSE shortening that resembles an accretionary wedge (related to an incipient subduction?) (Fig. 1). In central northern Venezuela, the San Sebastián Fault (Figs. 1 and 2), running along the coast, is responsible for most of the displacement; in eastern northern Venezuela, the El Pilar Fault, which separates the Araya–Paria Peninsula from the Interior Range, is inferred to play the same role.

The upper kilometers of the simplified sections (Fig. 2) are based on surface data and seismic reflection profiles for both the offshore part and the foreland sedimentary basins. The geometry of deeper structures is more speculative. However, with respect to present-day tectonics, the El Pilar Fault system is proposed to have a northward dip as illustrated in Fig. 2. Prior to the eastward drift of the Antillean Arc, the northern South-America (passive) margin developed with NW-SE transform faults and E-W normal growth faults facing north (Stéphan et al., 1990); the El Pilar system could thus represent an inheritance of one of the later ones. It is also in agreement with crustal section modeled by Jácome et al. (2008) (Fig. 3). The recent activity of this major fault was shown by field survey on Pleistocene deposits along the fault (Vierbuchen, 1978; Macsotay, 1976, 1977; Campos, 1981; Beltrán et al., 1996, 1999), high resolution seismic profiles in the Cariaco Gulf (Van Daele et al., in press) and, overall, by seismicity (several historical major earthquakes damaging the city of Cumaná (Paige, 1930; Audemard, 1999, 2007). Detailed studies were conducted after the last major event which struck the city of Cariaco, located at the eastern end of the Gulf of Cariaco (Baumbach et al., 2004; Audemard, 2006). A recently performed high resolution seismic survey of the Gulf

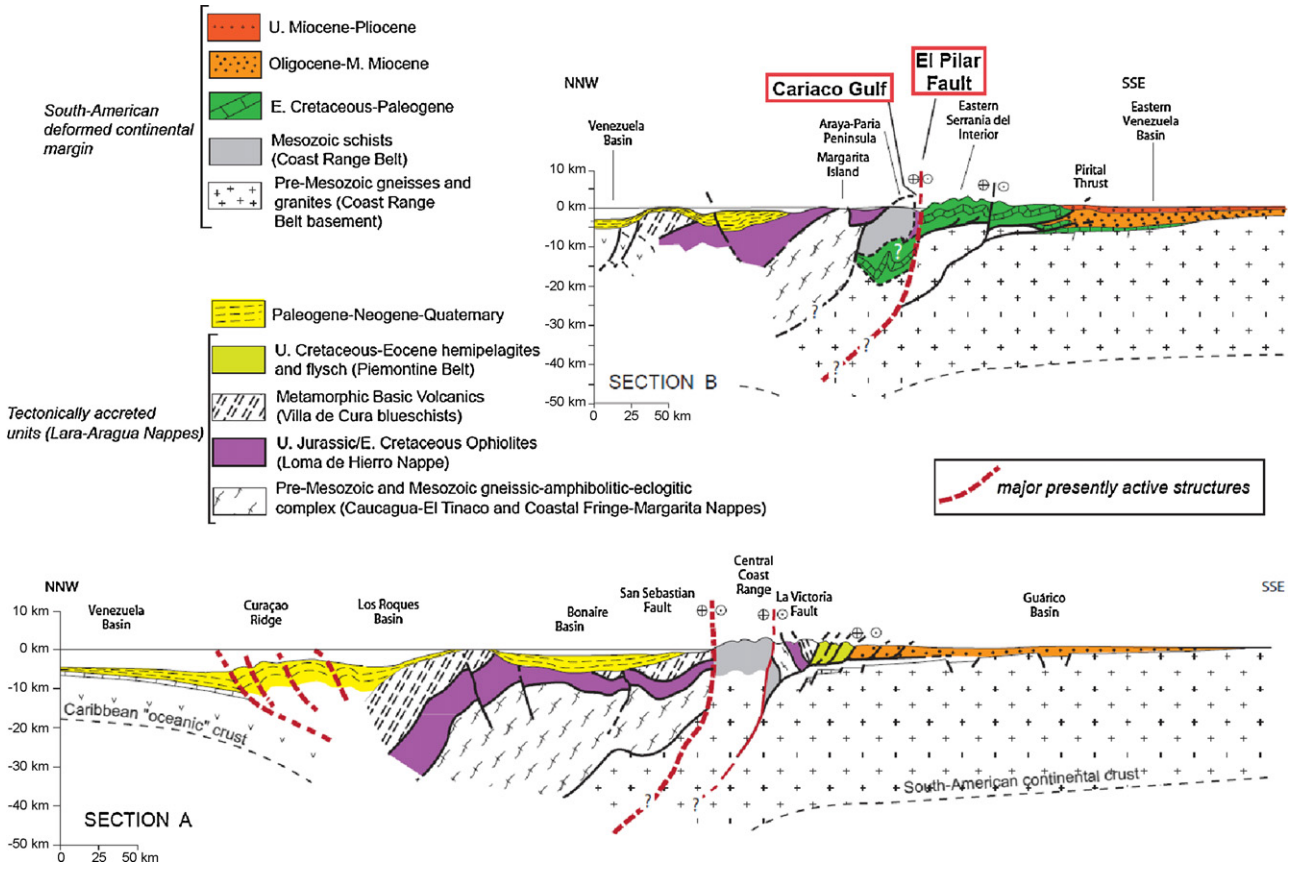

Fig. 2. Simplified sections across the southeastern Caribbean margin (based on maps and sections by Bellizzia et al. (1976), Stéphan et al. (1980), Campos (1981), Beck (1986), Chevalier (1987); locations in Fig. 1).

of Cariaco (Audemard et al., 2007) confirmed the importance of a major active trace bounding the southern coast of the gulf (Fig. 1), but also displayed older active traces along the northern gulf coast. As different works also evidenced other active faulting between the Araya Peninsula and the Island of Margarita (Pérez and Aggarwal, 1981), the seismic hazard assessment along the El Pilar Fault needs a precise knowledge of strain distribution between the Caribbean and South-America Plates. The global relative displacement is estimated to 20 mm/year (DeMets et al., 2000; Pérez et al., 2001a,b; Weber et al., 2001). Thus, our investigation program and GPS network were designed in order to study the major faults of the plate boundary.

Active tectonics and seismicity of the El Pilar Fault have been documented by trench excavations, revealing the occurrence of four earthquakes in the last 7–8 ka (Beltrán et al., 1996, 1999), and by historical records of destruction. Cumaná has been recurrently damaged, in 1530, 1684, 1766, 1797, 1853, 1929 and 1997 (Audemard, 1999). Reported impacts of the 1797 earthquake indicated the occurrence of a local earthquake, that might be similar to the 1929 earthquake that occurred east of Cumaná, whereas the 1766 earthquake has affected a larger area, suggesting an intermediate-depth earthquake. The 1530 and 1853 events, associated with tsunamis, are probably related to off-shore ruptures (Audemard, 2007). It must be underlined that there are no records of very large earthquakes during the last five centuries, which suggests that the segmentation of the fault by transpressional or transtensional relays reduces the size of the rupture area (Pérez and Aggarwal, 1981; Audemard, 2007). Focal mechanisms along the El Pilar Fault indicated right-lateral strike-slip on nearly vertical planes for earthquakes located in the upper crust (Baumbach et al., 2004; Audemard, 2006; Doser and Vandusen, 1996; Mendoza, 2000; Russo et al., 1993; Speed et al., 1991).

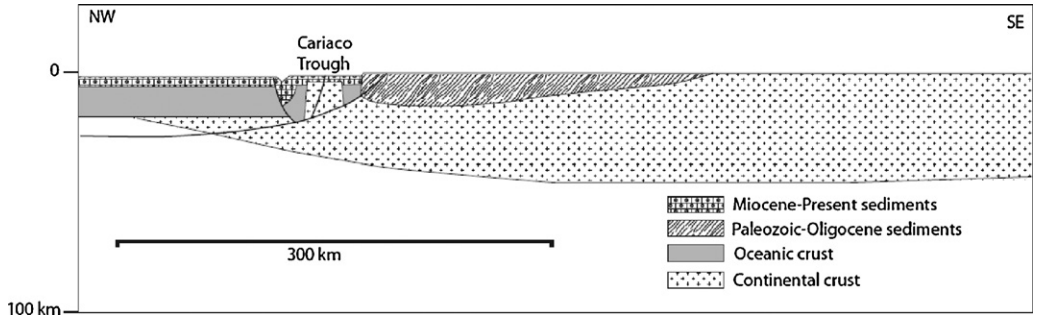

Fig. 3. Lithospheric cross section across the plate boundary from integrated seismic, flexural and gravity modeling (Jácome et al., 2008) at the level of the Cariaco Gulf.

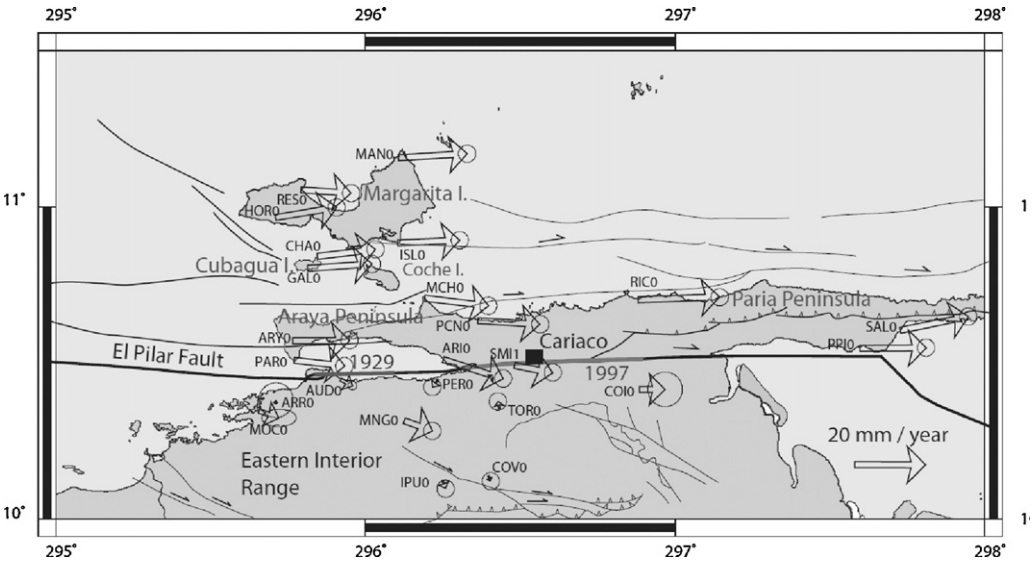

Fig. 4. Active faults in eastern Venezuela and velocities expressed in the South America plate reference frame, using the rotation pole proposed by Altamimi et al. (2007). Error ellipses are drawn for a 1σ confidence level assuming a flicker noise. Ruptures of the 1929 Cumaná and 1997 Cariaco earthquakes (Audemard, 2006) are indicated in grey.

1.3. The Central Range Fault in Trinidad

Geodetic investigations (Weber et al., 2009) and Neotectonics studies (Prentice et al., 2010; Soto et al., 2007) suggest that the principal fault of the plate boundary, west of Venezuela, in Trinidad Island is the Central Range Fault of Trinidad. Triangulation/GPS comparison between 1901–1903 and 1994–1995 allows to determine a velocity field suggesting that the Central Range Fault is the main structure of the plate boundary with a 12 ± 3 mm/year dextral strike-slip. It remains unclear if this fault is affected by a significant creep but it must be noticed that the preferred model of the authors suggest a fault with a 1–2 km locking depth. Nevertheless, no creep related offsets have been observed in the field (Prentice et al., 2010).

Neotectonic investigations indicate that the last earthquake along the Central Range Fault took place between 2710 and 550 yr BP which is in accordance with the lack of historical seismicity reported since 1800 for this fault.

2. Data collection

A dense GPS network (Fig. 4) has been installed and measured in December 2003 and re-measured in December 2005 using direct centering benchmarks. Each point has been measured during at least two sessions of 24 h, whereas one point, AUD0, was measured continuously during the full data acquisition program. Ashtech choke ring antennas were used during the two field acquisitions with ZXtrem Ashtech dual frequency receivers.

3. Data analysis

Results were obtained using IGS final precise orbits, as well as IGS Earth rotation parameters and data from nearby permanent GPS stations defined on the ITRF2005 reference frame. We used the absolute antenna phase center offsets models.

Data have been analyzed with the Bernese 5.0 software using the following strategy: (1) initial ionosphere-free analysis with residuals computation, (2) residuals analysis; (3) resolution of the wide-lane ambiguities using the Melbourne–Wubbena linear combination (Melboume, 1985; Wubbena, 1985); using DCB files when available, (4) computation of ionosphere free solution introducing the resolved Melbourne–Wubbena linear combination ambiguities, and (5) computation of normal equations. Troposphere-induced propagation delays were estimated from the observations every 2 h. Each daily solution has been transformed in the ITRF2005 reference frame (Altamimi et al., 2007) with a seven parameters Helmert solution using the IGS stations BOGT, BRAZ, BRMU, CHPI, CORD, CRO1, FORT, KOUR, PUR3, SSIA. Outliers detection has been performed with Bernese 5.0 software, using ITRF2005 sites coordinates and velocities constrained at their ITRF2005 values for points defined in the ITRF2005. The uncertainties estimated from this procedure assume a white noise source of error. It has long been recognized that the main source of error in GPS time-series is in fact a flicker noise (Zhang et al., 1997). Williams et al. (2004) have shown that flicker noise is a factor of 2–3 times higher than the corresponding white noise level. Based on that observation, we have increased our formal estimated error by a factor of 3.

Finally, we expressed velocities relative to the South America plate (Table 1 and Fig. 4) using the rotation pole between ITRF2005 and south America plate proposed by Altamimi et al. (2007). The influence of the choice of Altamimi's et al. rotation pole has been tested with others rotation poles (Drewes, 2009; Kreemer et al., 2003; DeMets et al., 2010) for selected points representing the network (Table 2). The tested models ITRF2005 (Altamimi et al., 2007), APKIM2005 (IGN) and APKIM2005 (DGF) (Drewes, 2009) and GSRM (Kreemer et al., 2003) are consistent for the east component at 0.2 mm/year and at 1.8 mm/year for the north component which is acceptable and smaller than error ellipses. The MORVEL (DeMets et al., 2010) model based on geological data differs significantly from the others models with differences reaching 1.2 mm/year for the east component and 3.3 mm/year for the north component. We have then adopt the ITRF2005 model as representative of most of the models, to express velocities in the South America reference frame.

4. Velocities field

Points located south of the network do not show significant velocities (2 ± 3 mm/year). Surprisingly, points TOR0, AUD0, PERO, and ARR0, located at a few kilometers south of the El Pilar Fault (Fig. 7), did not reveal significant velocities with respect to South America with a 3 mm/year uncertainty. The network south of the El Pilar fault presents then a 3 mm/year rigidity. A strong displace-

Table 1
Velocities in the ITRF2005 reference frame. Ve: east component of velocity, Vn: north component of velocity, σVe: standard deviation of Ve, σVn: standard deviation of Vn. Locations of stations in Fig. 4.

Station	Long (deg)	Lat (deg)	Ve (mm/year)	Vn (mm/year)	σVe (mm/year)	σVn (mm/year)
ARI0	−63.749	10.511	12.1	6.3	3	3
ARR0	−64.291	10.370	−4.7	12.6	6	6
ARY0	−64.236	10.571	11.3	11.8	3	3
AUD0	−64.081	10.447	−1.5	10	1.5	1.5
CHA0	−64.156	10.841	11.6	13.7	3	3
COI0	−63.116	10.415	2.5	11.8	6	6
COV0	−63.603	10.136	−4.1	10.4	3	3
GAL0	−64.188	10.802	13.4	13	3	3
HOR0	−64.291	10.965	12.4	14.6	3	3
IPU0	−63.751	10.122	−3.9	9.5	3	3
ISL0	−63.896	10.884	12.7	12.5	3	3
MAN0	−63.895	11.156	14.6	12.9	3	3
MCH0	−63.811	10.707	13.3	9.6	3	3
MNG0	−63.875	10.314	3.1	8.9	3	3
MOC0	−64.344	10.346	0.8	9.7	6	3
PAR0	−64.231	10.508	9.4	10.1	3	3
PCN0	−63.637	10.636	12.8	10.7	3	3
PER0	−63.767	10.446	−6.3	9.7	3	3
PPI0	−62.404	10.547	14	12	3	3
RES0	−64.209	11.053	9.3	10.8	3	3
RIC0	−63.120	10.701	18.3	12.6	3	3
SAL0	−62.274	10.604	14.5	15.8	3	3
SMI1	−63.519	10.492	6	9.7	3	3
TOR0	−63.569	10.352	−5.1	13.9	3	3

Table 2
Comparison of the velocity measured for the point IPU0 (southern part of the network), MAN0 (northern point of the network) and SAL0 (eastern point of the network) using different models of plate motion: ITRF2005 (Altamimi et al., 2007), APKIM2005 (IGN) and APKIM2005 (DGF) (Drewes, 2009), GSRM (Kreemer et al., 2003) and MORVEL (DeMets et al., 2010). Differences for the east component of velocity appear to be no larger than 0.2 mm/year excepted for the model MORVEL for which this difference reach 1.2 mm/year. Differences for the north component of velocity reach 1.8 mm/year between models ITRF2005, APKIM2005(IGN), APKIM2005(DGF), GRSM1.2, but this difference reach 3.3 mm/year for the model MORVEL that differs significantly from the others models.

	ITRF2005		APKIM2005 (IGN)		APKIM2005 (DGF)		GSRM v1.2		MORVEL	
	Ve	Vn	Ve	Vn	Ve	Vn	Ve	Vn	Ve	Vn
IPU0	0.85	−2.27	0.72	−1.77	1.06	−0.49	0.9	−0.64	1.98	1.04
MAN0	19.44	1.15	19.33	1.65	19.68	2.93	19.52	2.78	20.59	4.46
SAL0	19.23	3.9	19.11	4.36	19.46	5.64	19.3	5.48	20.39	7.15

ment gradient across a few kilometers is observed on both sides of the fault (thus on both sides of the Cariaco Gulf) which suggests a shallow locking depth or an aseismic component along the upper part of the El Pilar Fault. North of this strong gradient area, a regional gradient is documented up to Margarita island where velocity of 23 mm/year relative to South America is recorded for the RIC0 point located on the north coast of Araya–Paria peninsula. The asymmetry of displacement gradients on both sides of the El Pilar Fault suggests that the fault is not vertical at a lithospheric scale. Aseismic displacement could affect the ductile part of the El Pilar Fault dipping north below the Araya–Paria peninsula and the Margarita, Coche, Cubagua islands, as suggested by the cross-sections shown in Figs. 2 and 3 (Jácome et al., 2008). There is no clear evidence of current activity along the other strike-slip faults of the plate boundary (Fig. 4).

MNG0 point is affected by a significant eastward displacement whereas the others points of the Eastern Interior Range are not affected by such displacement. Possibly some instability in the site or the area/block which contains the monument may explain such anomalous displacement, we have not considered for modeling this suspicious point.

The lack of significant velocities for points IPU0, COV0 2 ± 3 mm/year located in the Eastern Interior Range relative to South-America plate clearly underlines the lack of significant velocities along the thrusts of the Eastern Interior Range over the Llanos (South America plate). The plate boundary is characterized by a pure dextral strike-slip solely along the El Pilar Fault.

5. Method displacement simulations

We used a set of dislocations in a uniform elastic half-space (Table 3) to simulate current velocities (Okada, 1985). We have used an inversion process based on an iterative least squares adjustments (up to 6 iterations) of free parameters as indicated in Table 3. The weighted differences between observed and simulated velocities using the Okada formulations of Green's functions have been minimized. We have minimized the number of free parameters using (1) geometrical constrains: the geometrical continuity between upper and deeper dislocations has been assumed, (2) geophysical constraints: the locking depth and the dip of the upper part of the fault have been determined with the distribution versus depth of microseismicity (Baumbach et al., 2004), (3) geological data: the location and orientation of the fault at surface have been determined by field data or high resolution seismic profiles (Van Daele et al., in press).

We have tested two categories of models: (i) with a unique El Pilar Fault segment, (ii) dividing the latter into two segments. Each segment, or sub-segment, is modeled following two dislocations: an upper one representing the upper and seismogenic part of the fault, where the slip may be locked, and a lower one affected by aseismic slip representing the part of the fault being in ductile conditions (Table 3). These two dislocations representing a segment of the fault have the same orientation and are connected at depth (Fig. 5).

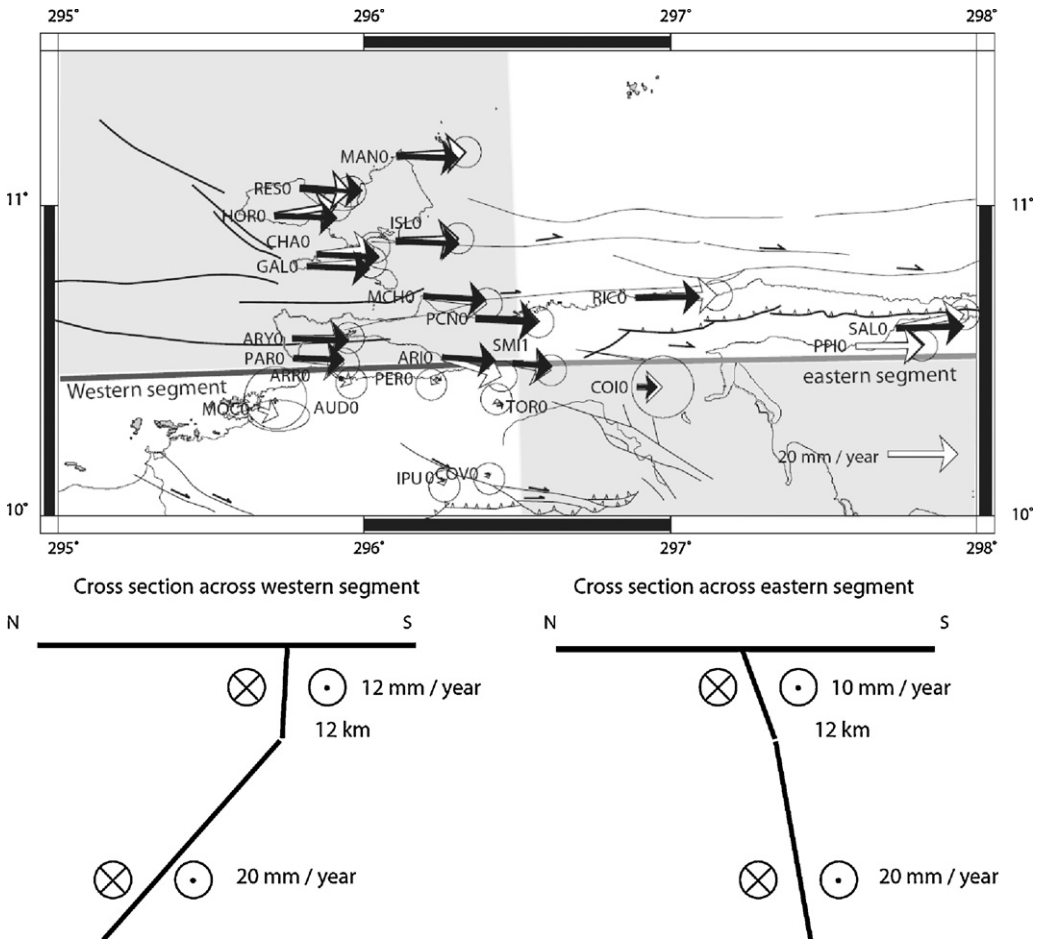

Fig. 5. Observed (white) and simulated (black) velocities using two segments (model 6) to represent the El Pilar Fault. Observed velocities are plotted in white with errors ellipses drawn for 66% confidence level and simulated velocities are plotted in black. Deep dislocations have been drawn by grey areas. Cross sections illustrate the change of dip for the deeper dislocations between eastern and western segments, probably due to inheritance from the normal fault stage of the El Pilar Fault when this margin was a passive margin, as well as the existence of an important aseismic slip along the upper part (0–12 km) of the fault.

The transition between the upper and lower dislocations has been fixed at 12 km according to the depth distribution of aftershocks (Baumbach et al., 2004). The location of the El Pilar has been determined with the precise location of the outcrops of the Fault. Strike-slip components along the upper dislocations have been determined through an inversion process, whereas the displacements rates along the deep dislocations have been fixed at a 20 mm/year dextral strike-slip component, representing the relative displacements between the Caribbean and South-America plates.

Several hypotheses were tested with one or two segments for the El Pilar Fault (2 or 4 dislocations) (Table 3), and the best fitting model has been chosen using the Fisher–Snedecor variances test (Table 3), that allows comparison of models with different degrees of freedom and to estimate the probability of differences between two compared models. To perform this test, we have supposed that the location and orientation of the two dislocations representing a fault segment can be considered as a single parameter set.

Models 4–6 (Table 3) incorporate two segments (Fig. 5) with two dislocations per segment, an upper nearly vertical dislocation between the surface and 12 km depth, and a lower dislocations plane face below 12 km. The dextral strike-slip component along the lower dislocations has been fixed at 20 mm/year whereas the displacement rates along the upper part of the fault were determined by the inversion.

6. Models comparison

Among the tests considering a single segment (Table 3), with one upper dislocation representing the seismogenic part of the fault (0–12 km depth), and one lower dislocation representing the deeper part of the fault supposed to be in ductile condition (thus affected by aseismic creep), the nearly vertical fault hypothesis used in previous studies (Pérez et al., 2001a,b) is probably not the best model as indicated by the Fisher–Snedecor test (Table 4). The model with a 70° northward dip of the lower dislocation is probably better (probability 60%) than this model. In any case, model 6 (Table 3), with two segments (4 non-vertical dislocations planes) appears better than model 1 with two vertical dislocations (Table 3).

The comparison of the two categories of models, one or two segments, through the Fisher test (Table 4), clearly demonstrates that models with two segments (models 5 and 6) are better than the best model with a single segment (model 2).

The maps of residuals for the models 1–6 (Fig. 6), clearly indicate that residual velocities for the models 1–4 are significantly greater than the residual velocities obtained for the model 5 and 6. Moreover, for the models 1–4 residuals present coherent tendencies, as by example un-modeled eastward velocities north of the fault and westward velocities south of it, which strongly suggested that these models are not satisfactory. The vertical fault hypothesis (model 1) does not allow to accurately model the recorded veloci-

Table 3
Summary of model parameters used to simulate velocities rates with a single segment (models 1–3) or two segments (models 4–6). The azimuth and surface location of the fault have been determined with geological information, the slip along the deeper part of the fault supposed to be in ductile condition has been fixed at 20 mm/year the total relative displacement between the Caribbean and the South America plates. We have supposed a geometrical continuity between the upper part (partially locked) and the deeper part of the fault. Parameters determined by the inversion are indicated by bold characters.

Model	Azimuth of the dislocation	Dip of upper part of the fault	Dextral strike-slip	Dip of lower part of the fault	Dextral strike-slip along the lower dislocation
1	88°	90°	**2.8 mm/year**	90°	20 mm/year
2	88°	90°	**2.9 mm/year**	70° northward	20 mm/year
3	88°	90°	**3.3 mm/year**	45° northward	20 mm/year

Model	Azimuth of segment 1	Dip of upper segment 1	Dextral strike-slip segment 1 upper	Dip of lower segment 1	Dextral strike-slip	Azimuth of segment 2	Dip of upper segment 2	Dextral strike-slip segment 2 upper	Dip of lower segment 2	Dextral strike-slip
4	87°	90°	**10 mm/year**	**50° northward**	20 mm/year	89°	90°	**3.5 mm/year**	**86° southward**	20 mm/year
5	88°	90°	**10 mm/year**	**32° northward**	20 mm/year	89°	90°	**3.5 mm/year**	**50° southward**	20 mm/year
6	88°	**87° northward**	**12 mm/year**	**53° northward**	20 mm/year	89°	**77° southward**	**10 mm/year**	**80° southward**	20 mm/year

Table 4
Selection of best model using Fischer–Snedecor test of variances to determine the probability for two models with different degrees of freedom to be significantly different. This test allows to compare models with a single fault (models 1–3), represent by two dislocations, with models with two segments of fault (models 4–6) represent by four dislocations and to select among these models the most probable one.

Model	*N* data	N parameters	Degree of freedom	χ^2
1	46	10	36	0.876
2	46	10	36	0.811
3	46	10	36	1.208
4	46	20	26	0.665
5	46	20	26	0.385
6	*46*	*20*	*26*	*0.319*

Comparison of models with Fisher–Snedecor test	Test	Probability	Results
Is model 2 better than model 1?	1.080	60%	Maybe
Is model 2 better than model 3?	1.490	89%	Yes
Is model 2 better than model 4?	1.135	65%	Maybe
Is model 5 better than model 2?	1.520	86%	Yes
Is model 6 better than model 2?	1.839	94%	Yes
Is model 6 better than model 5?	1.210	69%	Yes
Is model 6 better than model 4?	2.088	97%	Yes

ties as indicated by Fig. 6 and also by the projected velocities along a NS section as shown in Fig. 7.

We then modeled the El Pilar Fault as made of: a 50° northward dipping deep western segment, and an 80° southward dipping deep eastern segment (model 6). The upper part of the western segment is affected by a 12 mm/year displacement whereas the upper part of the eastern segment is affected by a 3–10 mm/year displacement (respectively model 5 and model 6 and Fig. 5). During the interseismic period, displacement along the upper, seismogenic part of the El Pilar is then modeled as 40% locked (12 mm/year of creep and 20–12 = 8 mm/year of locked displacement) for the western segment or at 50% (creep of 10 mm/year compared to 20 mm/year of relative velocity of Caribbean plate/South America plate) for the eastern segment (Fig. 5).

7. Interpretation

Our models show a good agreement between observed and simulated velocities, although only dislocations along the El Pilar Fault are taken into account. This implies that the relative displacements between the Caribbean plate and the South American plate are concentrated on the El Pilar Fault. There is then a lack of significant displacements along the other strike-slip faults in the plate boundary and a lack of significant shortening across the thrusts of the Serranía del Interior at present (Figs. 5 and 7).

This modeling also underlines the existence of important aseismic displacements along the upper part of the El Pilar Fault. Between 12 km depth and the surface, only 40% of displacement is locked for the western segment and 50% for the eastern segment.

The upper and seismogenic part of the fault, represented by the upper dislocations (Table 3), are nearly vertical for the two segments; our favoured solution is compatible with the published focal mechanisms indicating right-lateral strike-slip on nearly vertical planes for earthquakes located in the upper crust (Baumbach et al., 2004; Deng and Sykes, 1995; Doser and Vandusen, 1996; Mendoza, 2000; Russo et al., 1993; Speed et al., 1991). As an example, for the 1997 earthquake, the hypocenter depths were respectively estimated by the Bulletin ISC (BISC, 1998), by Pérez (1988), and by Romero et al. (1999), at 5 ± 2.3, 11 ± 1.5, and 9.4 km, whereas the aftershocks are located between the surface and 12 km depth (Baumbach et al., 2004). The main shock and the aftershocks are then all localised along the upper dislocation of the eastern segment.

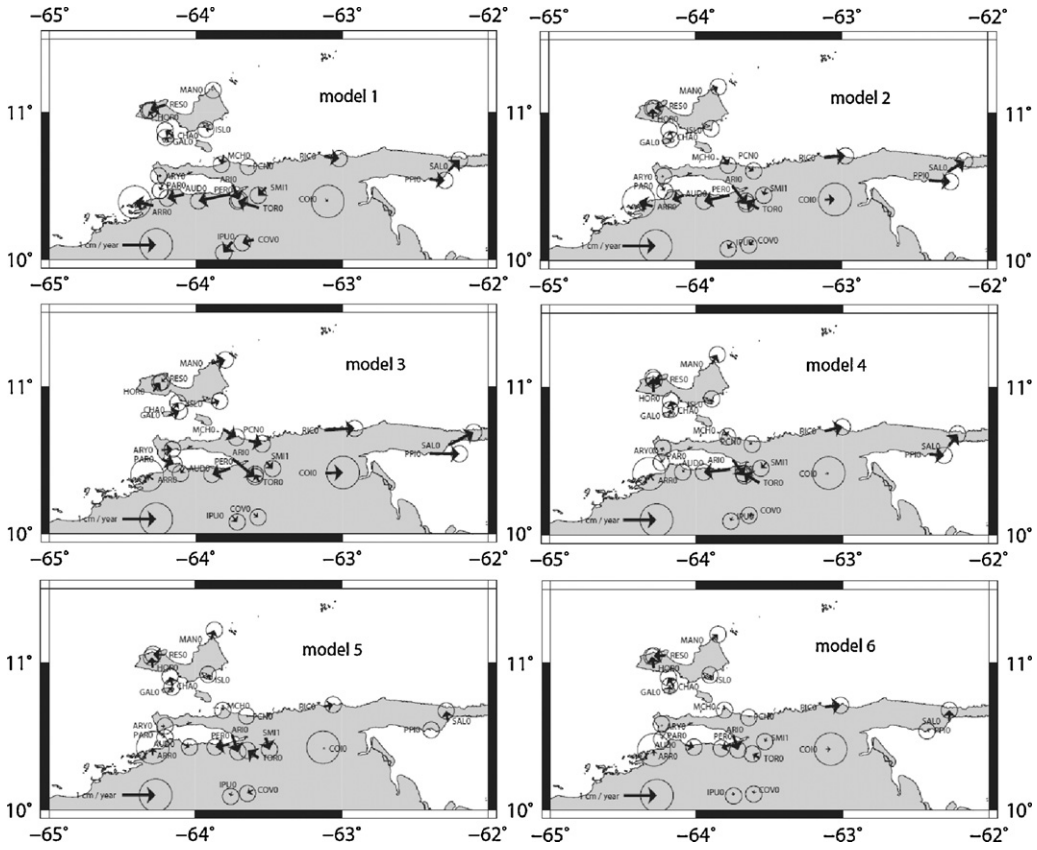

Fig. 6. Residuals between observed and modeled velocities for the 6 models present in this study. Models with two segments (models 4–6) representing the El Pilar fault are clearly better than models considering a single segment for the fault (models 1–3). Among the models considering that the El Pilar fault presents two segments, the model 6 is clearly the best: (1) residuals are less important than the residuals computed for the other models which is not the case for the model 4 by exemple, and (2) no clear tendency remains in the residual velocities.

7.1. Western segment

The model we favour for the western segment presents a 45° northward dipping lower dislocation (Table 3); this geometry reflects the geometry at depth of the western part of the EL Pilar Fault constrained by cross section. This geometry is an inheritance of a thrust fault related to the collision stage of the margin (Fig. 2). Asymmetric velocity field is then probably the result of this northward dipping lower segment and not the result of asymmetric distribution of material properties on each side of the fault, the

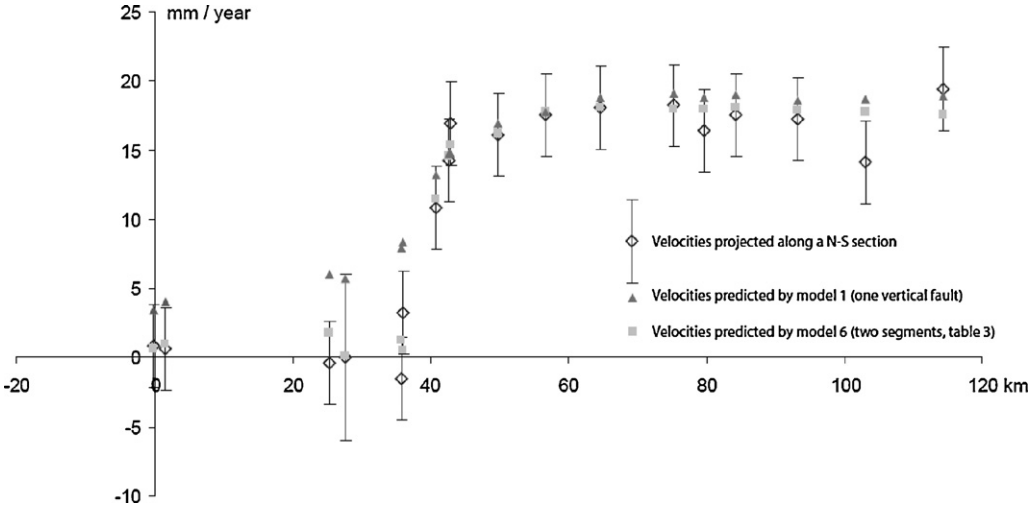

Fig. 7. E-W components of velocities with 1σ error bars projected along a NS cross sections and velocities simulated by the model 1 (vertical fault) and 6 (nearly vertical fault for the eastern segment, and fault dipping northward for the western segment). Points of the eastern part of the network (Paria peninsula) are not plotted on this figure. The model testing the hypothesis that the El Pilar fault is a vertical strike-slip fault (model 1) cannot simulated correctly the strong velocities gradient observed between the kilometer 25 and the kilometer 50, on the other hand, the model 6 considering a western part of the fault dipping northward presents a good adjustment between observed and simulated velocities. This model considers two segments, one eastern nearly vertical fault at depth, and one western segment for which the deeper part of the fault, below 12 km, dips northward.

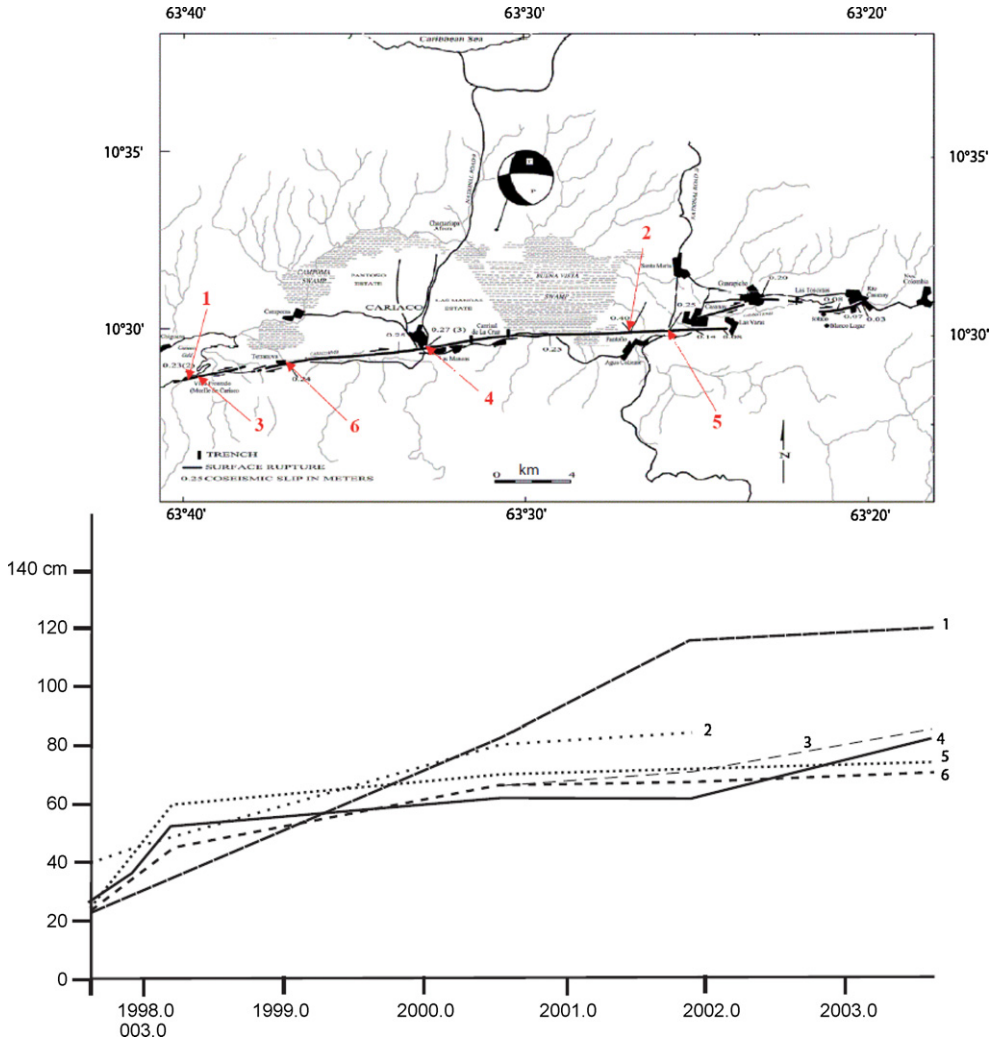

Fig. 8. Co and postseismic velocities measured by displaced markers (constructions, road border. . ..) along the surface fault trace between 1997 and 2003 illustrating the existence of localized aseismic displacement along the fault. No measurements are unfortunately available after 2003 but for numerous points, important postseismic displacements have ceased before the last measurement (points 1, 2, 5 and 6).

geological cross section supporting the existence of this northward dipping segment and not the existence of a major change of crustal thickness.

Aseismic displacements are not related to the post-seismic deformation after the 1997 earthquake as the western segment is mainly located west of the area affected by the earthquake. The western segment corresponds to the portion affected by the 1929 event and probably by the 1797 earthquake (Audemard, 2007). Consequently, a approximate 130-year-long return period can be preliminarily deduced between these two similar Ms 6.3 events. If we suppose a 30 km long rupture, a seismogenic part of the fault located between the surface and 13 km depth and a 3.1×10^{19} Pa s rigidity, each earthquake is associated at a 0.25 m coseismic earthquake. This value is clearly not compatible with a total locking of the El Pilar Fault (20 mm/year of slip deficit), and suggests the occurrence of important postseismic slips to be in accordance with the 8 mm/year slip deficit of our prefer model.

Creep in the upper part of the crust, has already been identified along major strike-slip faults including the San Andreas, Hayward and Calaveras faults in California (Steinbrugge et al., 1960; Rosen et al., 1998; Bürgmann et al., 1998, 2000; Lyons and Sandwell, 2003; Johansen and Bürgmann, 2005; Schmidt et al., 2005; Johansen et al., 2006), and the Ismetpasa segment of the North Anatolian fault in northern Turkey (Cakir et al., 2005). Since the western El Pilar Fault segment was affected by the 1929 Cumaná earthquake, two hypothesis are proposed to explain the creep of this segment: (1) the fault creep existed before the earthquake and the 1929 event has released stored strain; after a rapid rate of creep induced by the co-seismic strain release, the system has returned to the present-day rate of creep (2) the present-day creep is a post-seismic effect following the 1929 earthquake, after which the creep must continue to decrease with time, (3) the present-day creep is a post-seismic effect following the 1997 earthquake that affected laterally another segment of the fault. The presence of small serpentine bodies which have very low frictional coefficients (Moore et al., 1997) along this segment of the El Pilar Fault (Metz, 1965) could explain this behaviour. Similar behaviour was observed after two intermediate magnitude (ML 5.6 and 5.7) earthquakes on the Rodgers Creek Fault in California in 1969 and caused significant creep rates (Funning et al., 2007).

7.2. Eastern segment

The model we favour, for the eastern segment presents a lower dislocations dipping 80° southward (Table 3); we interpret this nearly vertical geometry as the tearing of the subducted oceanic lithosphere at the southern extremity of the Lesser Antilles subduction. At this particular point (Fig. 9, 3D sketch), the South-America

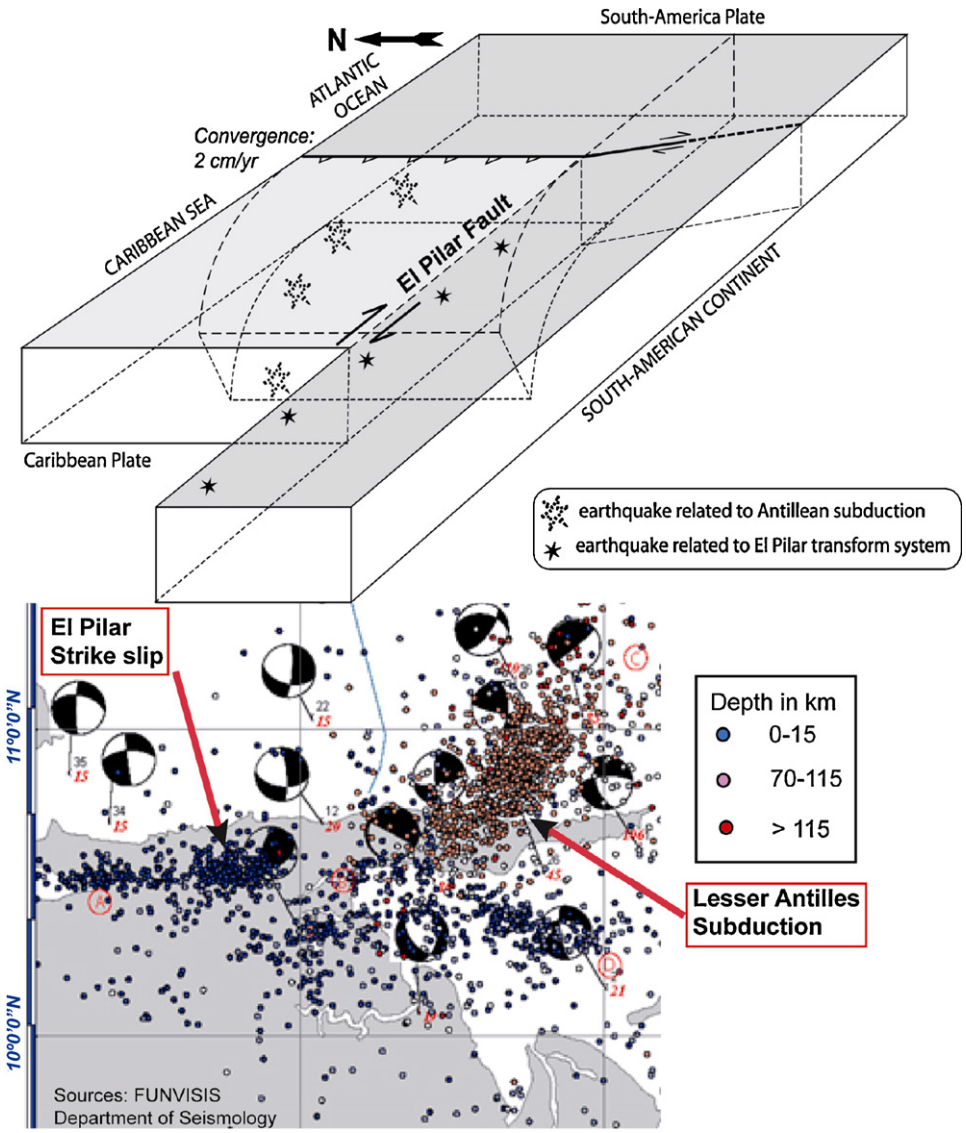

Fig. 9. Distribution of seismicity in eastern Venezuela and 3D scheme illustrating the existence of two distinct seismicities, a crustal seismicity located along the El Pilar Fault and its eastward prolongation and a deep one showing the southern limit of the West Indies subduction. The seismicity associated at the subduction abruptly ends along the eastern segment, probably nearly vertical, as determined by our preferred model, of the El Pilar Fault.

Plate gets torn into a subducted part (oceanic and marginal lithosphere) and a non-subducted part (continental lithosphere), the latter bounded by the El Pilar transform system. Microseismicity (Fig. 9, map), as well as few major earthquakes, fairly show this particular setting with two clearly separated zones: shallow foci along the El Pilar Fault, besides deep foci underlining subduction. The western part of the eastern segment coincides with the rupture of the 1997 earthquake, aseismic displacement may be then related to the occurrence of after-slip following this event as suggested by the occurrence of important aseismic displacements observed on the field along the fault trace (Audemard, 2006) and Fig. 8 during the first year after the earthquake. This localized after-slips triple (Fig. 8) the observed coseismic displacements during the 5 years following the 1997 Cariaco earthquake (Audemard, 2006). Postseismic moment release is then at least as important as the coseismic moment release as also observed for the co and postseismic slip associated with the 2004 Parkfield earthquake (Johansen et al., 2006). The postseismic after-slip along the San Andreas fault near Parkfield requests frictional parameters compatible with the experimental values obtained for serpentinites (Johnson et al., 2006). As shown in Fig. 8, surface after-slips following the 1997 earthquake determined by markers displacements, such as road borders, construction... are mainly important during the first months followings the earthquake. After these first months, localized surface displacements decreased (points 5 and 6), or present variations through time with local acceleration (points 3 and 4) during the last time span. These anthropogenic benchmarks are unfortunately not measurable any more.

It is then possible that during the 2003–2005 time span, simulated aseismic displacements reveal the occurrence of postseismic displacements or the occurrence of partial locking of displacement during interseismic period.

The existence of creep along the Caribbean–South America plate boundary is consistent with the preferred model of Weber et al. (2009) that proposes to simulate the velocities field in Trinidad, in both sides of the Central Range Fault with a single-fault elastic dislocation locked below 1–2 km and affected by a 12 ± 3 mm/year dextral strike-slip. In this hypothesis, the Central Range Fault would be affected by a creep in an interseismic period as shown by the lack of earthquake during the last 550 years (Prentice et al., 2010).

Once again this specific behaviour of the eastern segment of the El Pilar Fault may be related to the existence of serpentinites

bodies along the fault; deep-seated fluid-escaping could represent an alternate or additional factor.

If we consider the 1997 earthquake as a reference which seems to be reasonable as no larger earthquake has been found by neotectonics analysis and in historical seismicity (Audemard, 2007), it has been associated at a 1.3 m coseismic slip (Baumbach et al., 2004). If we consider that all the displacement (20 mm/year) is locked during interseismic period, a slip deficit corresponding at 1.3 m is obtained after 65 years only, we must then expect such earthquake each 65 years, which is clearly not observed in the historical seismicity.

If we suppose, on the contrary, that coseismic slip is followed by an important postseismic that triples the slip as observed in the field (Fig. 8), a characteristics earthquake would be associated to a 3.9 m slip. Such slip would be associated to a 195 years time span between similar earthquakes if the fault is completely locked, or at a 390 years time span is the fault is only 50% locked. The 1684 earthquake seems to be the precursor of the 1997 earthquake (Audemard, 2007) the recurrence time of earthquakes along this segment would be 313 years moreover neotectonic investigations based on four trenches analysis on this segment of the El Pilar fault indicate a 300–430 yeas time span between magnitude 7 earthquakes during the last 5600 years (Audemard, 2010). These observations clearly reinforce the hypothesis of a fault with important postseismic slip and a partial locking of displacement during interseismic period.

8. Conclusion

Within the surveyed area, the El Pilar Fault probably concentrates all the relative displacement between Caribbean and South America plates, as illustrated by the simulation of GPS velocities with only dislocations representing this fault. The Eastern Interior Range does not experience significant displacement relative to the South-America plate.

Velocities simulations using dislocations in a uniform elastic half space underline that the El Pilar Fault is nearly vertical only on the upper 12 km. Our prefer model suggests that a $\sim 50^{\circ}$ northward-dipping dislocations represents the lower part of western segment of the fault which seems to be an inheritance from a previous normal fault. In the case of the lower part of the eastern segment of the fault a 80° southward dipping dislocation is expected.

Modeling also underlines the existence of important creep (12 mm/year) along the upper part (0–12 km) of the western segment, where only 40% of displacement is locked in this seismogenic part of the fault. This specific behaviour also identified along Californian faults or along segment of the north Anatolian fault, is probably related to the existence of serpentinite bodies along the fault zone as observed in the herein-studied eastern segment of the fault, although, along the El Pilar Fault, abundant fluid-escapes (water, mud, gas) may also contribute to this behaviour as shown by the existence of several hot springs active along the southern coast of the Cariaco Gulf.

The upper part of the eastern segment is also affected by important 10 mm/year displacement, which may correspond to the existence of postseismic after-slip following the 1997 Cariaco earthquake or at a partial locking during interseismic period. With as much as half locking of the displacement, this could also be related to the existence of serpentinite bodies along the fault plane.

Acknowledgments

The authors wish also to thank John Weber and an anonymous reviewers for their helpful comments and suggestions.

Both data acquisition campaigns (2003 and 2005) have been carried out with a pool of instruments from INSU to which we are much indebted. Pierre Briole is thanked for allowing the use of the inversion software. We would like to thank the financial and logistic support offered by FUNVISIS and LGCA-Université de Savoie. Part of this research was possible thanks to the financing by the DyETI programme. Particular thanks in Venezuela go to Nuris Orihuela and Gustavo Malavé (former presidents of FUNVISIS) and the following personnel: José Antonio Rodríguez, Victor Cano, Luis Melo (now at PDVSA-Oriente), Michel Bechtold (Germany; at internship at FUNVISIS), Javier Sánchez and Fabian Rada, who carried out the fieldwork with the authors. Special thanks are for Geol. Melo for helping in the making of the spits and their final installation on a large number of the chosen localities. These campaigns could not have been possible without the help of all locals from all over eastern Venezuela who watched over the equipments every single night. At our central station/main camp we wish to thank the Audemard family for unconditional permit and their undless hospitality; and especially to our ever-ready on-site hosts (also cook, watchmen, and bartenders) Luis José "Pinche" Hernández and wife Luisa. Permit and logistic support from PDVSA-Oriente (at Guaraguao), particularly from José Borrego, are much appreciated. This research is a contribution to projects FONACIT 2002000478 (GEODINOS) and FONACIT-ECOS Nord PI-2003000090 (French code: VU4001).

References

Bellizzia, A., Pimentel, N., Bajo de Osuna, R., 1976. Mapa geológico-estructural de Venezuela. Scale 1: 500.000. Ministerio de Minas e Hidrocarburos. – Ed. Foninves. Caracas.

González de Juana, C., Iturralde de Arozena, J.M., Picard Cadillat, X., 1980. Geología de Venezuela y de sus cuencas petroliferas. Ed. Foninves, Caracas, 2 vol., 1031 pp.

Hackley, P.C., Urbani, F., Karlsen, A.W., Garrity, P.C., 2005. New geologic shaded relief map of Venezuela at 1:750 000 scale. Open-file Report 2005-1038. U.S. Geological Survey, 2 sheets.

Peirson, A.L., 1965. Geology of the Guárico Mountain Front. Boletín informativo de la Asociación Venezolana de Geología. Minería y Petróleo 8 (7), 183–212.

Menéndez, A., 1966. Tectónica de la parte central de las Montañas Occidentales del Caribe. Venezuela. Boletín de Geología, Ministerio de Minas de Venezuela, XIII, vol. 15, pp. 116–140.

Bell, J., 1971. Tectonic evolution of the Central Part of the Venzuelan Ranges. Bulletin Geological Society of America 130, 107–118.

Bellizzia, A., 1972. Sistema Montañoso del Caribe. borde Sur de la Placa Caribe? Es una cordillera alóctona? Memorias IV Conferencia Geológica del Caribe, Margarita, Venezuela, pp. 247–258.

Stéphan, J.-F., 1985. Andes et Chaîne Caraïbe sur la Transversale de Barquisimeto (Venezuela). Evolution géodynamique. In: Mascle, A. (Ed.), Caribbean Geodynamics, Ed. Technip, Paris, pp. 505–529.

Beck, C., 1985. Las Napas de Aragua -Cadena Caribe Central- y la historia Mesozoica del margen Sur del Caribe a lo largo del meridiano de Caracas. In: Mascle, A. (Ed.), Caribbean Geodynamics, Ed. Technip, Paris, pp. 541–551.

Rod, E., 1956. Strike-slip faults of northern Venezuela. American Association of Petroleum Geologists Bulletin 40, 457–476.

Stéphan, J.-F., Mercier de Lépinay, B., Calais, E., Tardy, M., Beck, C., Carfantan, J.-C., Olivet, J.-L., Vila, J.-M., Bouysse, P., Mauffret, A., Bourgois, J., Théry, J.-M., Tournon, J., Blanchet, R., Dercourt, J., 1990. Paleogeodynamic maps of the Caribbean: 14 steps from Lias to Present. Bulletin de la Société Géologique de France 8 (VI), 915–919, 14 appendices.

Graterol, V., 1988. Mapa de anomalía de Bouguer de la República de Venezuela. Escala 1:2.000.000. Univ. Simón Bolívar y Ministerio del Ambiente y Recursos Renovables.

Vignali, M., 1977. Geology between Casanay and El Pilar (El Pilar Fault zone). Estado Sucre, Venezuela. Abstracts VIIIth Caribbean Geological Conference, Curaçao, pp. 215–216.

Vierbuchen, R., 1978. Geology of the El Pilar Fault region, State of Sucre, and its tectonic implications. Ph.D. Thesis, University of Princeton, 169 pp.

Beck, C., Ogawa, Y., Dolan, J., 1990. Eocene paleogeography of the southeastern Caribbean: relations between sedimentation on the Atlantic abyssal plain at O.D.P. Site 672 and evolution of the South-America margin. In: Proc. O.D.P. Sci. Results, College station, TX (Ocean Drilling Program), vol. 110, pp. 7–16.

DeMets, C., Jansma, P.E., Mattioli, G.S., Dixon, T.H., Farina, F., Bilham, R., Calais, E., Mann, P., 2000. GPS geodetic constraints on Caribbean-North America plate motion. Geophysical Research Letters 27 (3), 437–440.

Minster, J., Jordan, T., 1978. Present-day plate motions. Journal of Geophysical Research 83, 5331–5354.

Pérez, O., Aggarwal, Y., 1981. Present-day tectonics of southeastern Caribbean and northeastern Venezuela. Journal of Geophysical Research 86, 10,791–10,805.

Audemard, F.A., Machette, M., Cox, J., Hart, R., Haller, K., 2000. Map of Quaternary Faults of Venezuela. Scale 1:2,000,000; jointly published with Database of Quaternary Faults in Venezuela and Offshore regions (USGS Open-File Report 00-18; 78 p). A project of the International Lithosphere Program Task Group II-2: Major active Faults of the World (Regional Coord.: Carlos Costa. Univ. San Luis-Argentina; ILP II-2 cochairman Western Hemisphere: Michael Machette. USGS-Colorado). Also available from USGS web page. Reprinted as a FUNVISIS Anniversary special edition.

Pérez, O.J., Bilham, R., Bendick, R., Hernández, N., Hoyer, M., Velandia, J., Moncayo, C., Kozuch, M., 2001a. Velocidad relativa entre las placas del Caribe y Sudamérica a partir de observaciones dentro del sistema de posicionamiento global (GPS) en el norte de Venezuela. Interciencia 26 (2), 69–74.

Pérez, O.J., Bilham, R., Bendick, R., Velandia, J.R., Hernandez, N., Moncayo, C., Hoyer, M., Kozuch, M., 2001b. Velocity field across the southern Caribbean plate boundary and estimates of Caribbean/South-American plate motion using GPS geodesy 1994–2000. Geophysical Research Letters 28, 2987–2990.

Weber, J., Dixon, T., DeMets, C., Ambeh, W., Jansma, P., Mattioli, G., Saleh, J., Sella, G., Bilham, R., Pérez, O., 2001. GPS estimate of relative motion between the Caribbean and South American plates and geologic implications for Trinidad and Venezuela. Geology 29 (1), 75–78.

Jácome, M.I., Rondón, K., Schmitz, M., Izarra, C., Viera, E., 2008. Integrated seismic. Flexural and gravimetric modelling of the Coastal Cordillera Thrust Belt and the Guárico Basin, North-Central Region, Venezuela. Tectonophysics, doi:10.1016/j.tecto.2008.03.008.

Macsotay, O., 1976. Bioestratigrafía de algunas secciones pleistocenas del nororiente de Venezuela. Boletín de Geología, Publ. Esp., Caracas 7 (2), 985–996.

Macsotay, O., 1977. Observaciones sobre el neotectonismo Cuaternario en el nororiente Venezolano. Boletín de Geología, Publ. Esp., Caracas 7 (3), 1861–1883.

Campos, V., 1981. Une transversale de la Chaîne Caraïbe et de la marge vénézuélienne dans le secteur de Carúpano (Vénézuela oriental): structure géologique et évolution géodynamique. Ph.D. Thesis. Western Bretagne University, Brest, 160 pp.

Beltrán, C., Singer, A., Rodríguez, J.A., 1996. The El Pilar fault active trace (northeastern Venezuela): neotectonic evidences and paleoseismic data. In: 3rd International Symposium on Andean Geodynamics, Saint-Malo, France, pp. 153–156.

Beltrán, C., Rodríguez, J.A., Singer, A., Rivero, C.A., 1999. La trinchera de Las Toscanas. Evidencias paleosismológicas de actividad reciente de la falla de El Pilar entre Casanay y Río Casanay. Venezuela. VI Congreso Venezolano de Sismología e Ingeniería Sísmica, Mérida, Venezuela (CD-ROM format).

Van Daele, M., Van Welden, A., Moernaut, J., Beck, C., Audemard, F., Sanchez, J., Jouanne, F., Carrillo, E., Malavé, G., Lemus, A., De Batist, M., 2010. Reconstruction of Late Quaternary sea- and lake-level changes in a tectonically active marginal basin using seismic stratigraphy: the Gulf of Cariaco, NE Venezuela. Marine Geology.

Paige, S., 1930. The Earthquake at Cumaná, Venezuela, January 17, 1929. Bulletin of the Seismological Society of America 20 (12), 1–10.

Audemard, F.A., 1999. Nueva percepción de la sismicidad histórica del segmento en tierra de la falla de El Pilar. Venezuela nororiental. A partir de primeros resultados paleosísmicos. In: Proceedings VI Congreso Venezolano de Sismología e Ingeniería Sísmica, Mérida, 10 pp (in CD-ROM).

Audemard, F.A., 2007. Revised seismic history of the El Pilar fault. Northeastern Venezuela. From the Cariaco 1997 earthquake and recent preliminary paleoseismic results. Journal of Seismology 11 (3), 311–326.

Baumbach, M., Grosser, H., Romero, G., Rojas, J., Sobiesiak, M., Welle, W., 2004. Aftershock pattern of the July 9. 1997. Mw = 6.9 Cariaco earthquake in Northeastern Venezuela. Tectonophysics 379, 1–23.

Audemard, F.A., 2006. Surface rupture of the Cariaco July 09, 1997 Earthquake on the El Pilar fault, northeastern Venezuela. Tectonophysics 424, 19–39.

Audemard, F.A., Beck, C., Moernaut, J., De Rycker, K., De Batist, M., Sánchez, J., González, M., Sánchez, C., Versteeg, W., Malavé, G., Schmitz, M., Van Welden, A., Carrillo, E., Lemus, A., 2007. La depresión de Guaracayal. estado Sucre. Venezuela: una cuenca en tracción que funciona como barrera para la propagación de la ruptura cosísmica. Interciencia 32 (11), 735–741.

Deng, J., Sykes, R.S., 1995. Determination of Euler pole for contemporary relative motion of Caribbean and North American plates using slip vectors of interplate earthquakes. Tectonics 14, 39–53.

Doser, D.I., Vandusen, S.R., 1996. Source process of large (Mz6.5) earthquake of the southeastern Caribbean (1926–1960). Pure Applications and Geophysics 146, 43–66.

Mendoza, C., 2000. Rupture history of the 1997, Cariaco, Venezuela earthquake from teleseismic P-waves. Geophyical Research Letters 27, 1555–1558.

Russo, R.M., Speed, R.C., Okal, E.A., Shepherd, J.B., Rowley, K.C., 1993. Seismicity and tectonics of the southeastern Caribbean. Journal of Geophysical Research 98, 14299–14319.

Speed, R., Russo, R., Weber, J., Rowley, K.C., 1991. Evolution of southern Caribbean plate boundary, vicinity of Trinidad and Tobago: discussion. American Association of Petroleum Geologists Bulletin 75 (11), 1789–1794.

Weber, J.C., et al., 2009. Triangulation-to-GPS and GPS-to-GPS geodesy in Trinidad, West Indies: Neotectonics. Marine and Petroleum Geology, doi:10.1016/j.marpetgeo.2009.07.010.

Prentice, C.S., Weber, J.C., Crosby, C.J., Ragona, D., 2010. Prehistoric earthquakes on the Caribbean–South American plate boundary, Central Range fault, Trinidad. Geology 38, 675–678.

Soto, M.D., Mann, P., Escalona, A., Wood, L.J., 2007. Late Holocene strike-slip offset of a subsurface channel interpreted from three-dimensional seismic data, eastern offshore Trinidad. Geology 35 (9), 859–862.

Melbourne, W.G., 1985. The case for ranging in GPS based geodetic systems. In: Goad, C. (Ed.), Proc. 1st Int. Symp. On Precise Positioning with the Global Positioning System. US Department of Commerce, Maryland, USA, pp. 373–386.

Wübbena, G., 1985. Software developments for geodetic positioning with GPS using TI4100 code and carrier measurements. In: Goad, C. (Ed.), Proc. 1st Int. Symp. On Precise Positioning with the Global Positionning System. US Department of Commerce, Maryland, USA, pp. 403–412.

Altamimi, Z., Collilieux, X., Legrand, J., Garayt, B., Boucher, C., 2007. ITRF2005: a new release of the international terrestrial reference frame based on time series of station positions and earth orientation parameters. Journal of Geophysical Research 112, B09401, doi:10.1029/2007JB004949/.

Zhang, J., Bock, Y., Johnson, H., Fang, P., Genrich, J.F., Williams, S., Wdowinski, S., Behr, J., 1997. Southern California permanent GPS geodetic array: error analysis of daily position estimates and site velocities. Journal of Geophysical Research 102 (18), 035-18 055. doi:10.1029/97JB01380.

Williams, S.D.P., Bock, Y., Fang, P., Jamason, P., Nikolaidis, R.M., Prwirodirdjo, L., Miller, M., Johnson, D.J., 2004. Error analysis of continuous GPS position time series. Journal of Geophysical Research 109 (B3), B03412, doi:10.1029/2003JB002741.

Drewes, H., 2009. The actual plate kinematic and crustal deformation model APKIM2005 as basis for a non-rotating ITRF. In: Drewes, H. (Ed.), Geodetic reference frames, International Association of Geodesy Symposia 134. doi:10.1007/978-3-642-00860-3_15, Springer–Verlag, Berlin, Heidelberg.

Kreemer, C., Holt, W.E., Haines, A.J., 2003. An integrated global model of present-day plate motions and plate boundary deformation. Geophysical Journal International 154, 8–34.

DeMets, C., Gordon, R.G., Argus Donald, F., 2010. Geologically current plate motions. Geophysical Journal International 181, 1–80, doi:10.1111/j.1365-246X.2009.04491.x.

Okada, Y., 1985. Surface deformation due to shear and tensile faults in a half-space. Bulletin of the Seismological Society of America 75 (4), 1135–1154.

Bulletin of the International Seismological Center, 35, 123 (November/December), 1998.

Pérez, O.J., 1988. Seismological report on the Mw = 6.8 strong shock of 9 July 1997 in Cariaco, northeastern Venezue48la. Bulletin of the Seismological Society of America 88, 874–879.

Romero, G., Audemard, F., Schmitz, M., Rendõn, H., 1999. The July 9, 1997 Cariaco earthquake, Venezuela: correlation between aftershock distribution and surface rupture. Eos Trans. AGU 80 (27), Spring Meet. Suppl., Abstract S42A-04, 1999.

Steinbrugge, K.V., Zacher, E.G., Tocher, D., Whitten, C.A., Clair, C.N., 1960. Creep on the San Andreas fault. Bulletin of the Seismological Society of America 50, 396–404.

Rosen, P., Werner, C., Fielding, E., Hensley, S., Buckley, S., Vincent, P., 1998. Aseismic creep along the San Andreas fault Parkfield, CA measured by radar interferometry. Journal of Geophysical Research 25, 825–828.

Bürgmann, R., Fielding, E., Sukhatme, J., 1998. Slip along the Hayward fault, California, estimated from space-based synthetic aperture radar interferometry. Geology 26, 559–562.

Bürgmann, R., Schmidt, D., Nadeau, R.M., d'Alessio, M., Fielding, E., Manaker, D., McEvilly, T.V., Murray, M.H., 2000. Earthquake potential along the northern Hayward fault, California. Science 289, 1178–1181.

Lyons, S.N., Sandwell, D.T., 2003. Fault-creep along the southern San Andreas from InSAR, permanent scatterers, and stacking. Journal of Geophysical Research 108, doi:10.1029/2002JB001831.

Johansen, I.A., Bürgmann, R., 2005. Creep and quakes on the northern transition zone of the San Andreas fault from GPS and InSAR data. Geophysical Research Letters 32, L14306, doi:10.1029/2005GL023150.

Schmidt, D.A., Bürgmann, R., Nadeau, R.M., d'Alessio, M.A., 2005. Distribution of aseismic slip-rate on the Hayward fault inferred from seismic and geodetic data. Journal of Geophysical Research 110, B08406, doi:10.1029/2004JB003397.

Johansen, I.A., Fielding, E.J., Rolandone, F., Bürgmann, R., 2006. Coseismic and postseismic slip of the 2004 Parkfield earthquake from space-geodetic data. Bulletin of the Seismological Society of America 96, 269–282.

Cakir, Z., Akoglu, A.M., Belabbes, S., Ergintav, S., Meghraoui, M., 2005. Creeping along the Ismetpasa section of the North Anatolian fault (Western Turkey): rate and extent from InSAR. Earth and Planetary Science Letters 238, 225–234.

Moore, D., Lockner, D.A., Shengli, M., Summers, R., Byerlee, J., 1997. Strengths of serpentinite gouges at elevated temperatures. Journal of Geophysical Research 102, 14787–14801.

Metz, H., 1965. Geology of the El Pilar Fault Zone. State of Sucre, Venezuela. IV Caribbean Geological Conference, Trinidad, pp. 293–298.

Funning, G., Bürgmann, R., Ferretti, A., Novali, F., Fumagalli, A., 2007. Creep on the Rodgers Creek fault from PS-InSAR measurements. Geophysical Research Letters 34, doi:10.1029/2007GL030836R.

Johnson, K.M., Bürgmann, R., Larson, K., 2006. Frictional on the San Andreas fault near Parkfield, California, inferred from models of afterslip following the 2004 earthquake. Bulletin of the Seismological Society of America 96, 321–338.

Audemard, F.A., 2010 Multiple trench investigation across the newly ruptured segment of the El Pilar fault in northeastern Venezuela, after the Cariaco 1997

earthquake. In: Audemard, F.A., Michetti, A., McCalpin, J. (Guest editors), Geological Criteria for Evaluating Seismicity Revisited: 40 Years of Paleoseismic Investigations and the Natural Record of Past Earthquakes. GSA Special book.
Stéphan, J.-F., Beck, C., Bellizzia, A., Blanchet, R., 1980. La Chaîne Caraïbe du Pacifique à l'Atlantique. XXVIth International Geological Congress, Paris, c-5, pp. 38–59.
Beck, C., 1986. Géologie de la Chaîne Caraïbe au méridien de Caracas (Vénézuela). Mémoire Soc. Géol. Nord. Lille, 460 pp.
Chevalier, Y., 1987. Les zones internes de la Chaînes Sud-Caraïbe sur le transect Ile de Margarita-Péninsule d'Araya. (Vénézuela). Ph.D. Thesis. Western Bretagne University, Brest, 504 pp.